# Three-dimensional transverse vibration of microtubules

Si Li, Chengyuan Wang*, Perumal Nithiarasu

Zienkiewicz Centre for Computational Engineering, College of Engineering, Swansea University, Bay Campus, Fabian Way, Swansea, Wales SA1 8EN, UK

**Abstract** A three-dimensional (3D) transverse vibration was reported based on the molecular structural mechanics (MSM) model for microtubules (MTs), where the bending axis of the cross section rotates in an anticlockwise direction and the adjacent half-waves oscillate in different planes. Herein, efforts were invested to capturing the physics behind the observed phenomenon and identifying the important factors that influence the rotation angle between adjacent two half waves. A close correlation was confirmed between the rotation of the oscillation planes and the helical structures of MTs, showing that the 3D mode is a result of the helicity found in MTs. Subsequently, the wave length-dependence and the boundary condition effects were also investigated for the 3D transverse vibration of MTs. In addition, the vibration frequency was found to remain the same in the presence or absence of the bending axis rotation. This infers that the unique vibration mode is merely due to the bending axis rotation of the cross section but no significant torsion occurs for MTs.

**Keywords:** Microtubules; three-dimensional transverse vibration; Helical structure; structure mechanics model

---

*Corresponding author. E-mail address: chengyuan.wang@swansea.ac.uk (C. Wang)

## 1. Introduction

Microtubules (MTs), as structural and functional components of cells, can maintain the cell shapes, generate the cell rigidity, provide tracks for molecular motors to transport organelles and facilitate the inter-cellular mobility and many other physiological processes [1]. The basic components of MTs are α–β heterodimers [2], which stack head to tail to form the protofilaments (PFs). MTs are finally constructed by a number of the PFs bonded laterally to form a cylindrical surface [3, 4]. MTs have various architectures characterized by the PF number $N$ and the helix-start number $S$. For most MTs, $N$=13 and $S$=3 [5], but those with $N$ = 8 to 16 and $S$ = 2 to 4 are also reported in the literature. In particular, the latter lead to misfit in MTs and accordingly, generate a skew angle between the PF and axis of the MTs. [6, 7].

As one of the fundamental structural elements in cells MTs can withstand external load, detect the mechanical changes in the cellular environment and organize the remodeling of the whole cytoskeleton [8, 9]. Thus the mechanics of MTs has excited extensive studies in the last two decades [10-14]. Specifically, the vibration of MTs has drawn considerable attention from the communities of nano and biomechanics [10-17] as it has the potential to impact on the intra-cellular physiological processes [18-21], provides a physical mechanism for the novel non-invasive biosensors [22] and facilitates the development of advanced biomimetic nanomaterials, e.g., MT-graphene nanotubes, whose applications rely heavily on MT vibration [23, 24].

Another fundamental issue in MT mechanics is the relation between the MT structures and their mechanical behavior and properties [25]. This however has not been examined in detail until a recent study on the elastic properties of MTs based on a recently developed molecular structural mechanics (MSM) model [15, 16, 26]. The possible reason is that the

previously used continuum models [12, 13] are unable to account for the structural details and the molecular dynamics simulations (MDS) [27] are computationally expensive for the analyses. This situation thus provides an impetus for us to further examine the possible structural effect on the vibration of MTs based on the MSM model [15, 16, 26], which enjoys highly improved efficiency as compared with MDS and largely enlarged scope relative to the continuum mechanics models.

In the present paper, the MSM model [15, 16, 26] was employed to investigate the beam-like bending vibration for MTs with an emphasis on its dependence on the structures and the geometric size of MTs. The layout of the paper is as follows. The MSM techniques and details of MT structures are introduced in Sec.2. Then Sec. 3 gives the description of the achieved novel vibration modes with the bending axis rotating on MT cross sections. It is followed by a discussion on the major factors that exert influence on the vibration mode. The new findings based on the results and discussions are summarized in Sec.4.

## 2. Methods

### 2.1 MT Structure and MSM model

As mentioned above, MTs are long tubular structures with neighboring *PF*s shifted relatively to each other longitudinally, which results in helical structures as shown in Fig. 1a, b and c [28]. Various architectures are found for MTs with the *PF* number $N$ varying from 8 to 17 and helix-start number $S$ changing from 2 to 4[28]. The most common configuration is the standard 13-3($N$=13 $S$=3) MTs [6, 7, 29]. Others are the non-standard MTs showing the misfit in MTs, which is compensated by skewing PFs relative to the axial direction [6, 7].

Fig. 1a-c showed the parameterized MTs structure characterized primarily by $N$ and $S$, which satisfy the equations below [7, 15, 16, 30]:

$$r=\frac{Sa}{N}-\delta x\tan(\theta)$$
$$R=\frac{Sa\tan(\theta)+N\delta x}{2\pi} \quad (1)$$

Herein $a$ is the subunit repeat, $r$ is the subunit rise, $R$ is the radius of the tube, $\delta x$ is the *PF* separation, and $\theta$ is the skew angle of *PF* relative to the direction of the rolling axis of MT. The values of *PF* separation, subunit repeat and skew angles of various MTs are present in Table1 and considered in the simulations of the present study.

To account for the structural details of MTs an MSM model[15] was developed for MTs. Similar techniques were also applied to the carbon nanotubes [31]. The MSM model was further employed in the present study due to its high computational efficiency and capability of accounting for the structural details of MTs. In particular, the MSM method was efficiently used to characterize the mechanical responses of MTs and found to be in good agreement with available experiments or atomistic simulations [15, 26].

The space structure of MTs was shown in Fig. 1d, where the intra-*PF* αβ interactions, i.e., bond1(represented by the blue lines in Fig.1c), are modeled as the elastic space beam 1 and the inter-PF αα (ββ) interaction, i.e., bond 2 (denoted by the red lines in Fig.1c), are treated as the elastic space beam 2. Following previous studies [15, 16, 32], the small difference in αα and ββ interactions is neglected. Such a frame structure consisting of the space beams is then obtained as an MSM model for an MT.

In the molecular mechanics, the force field is expressed in the form of steric potential energy. The major parts of the steric potential energy of an MT structure include the bond

stretching energy $U_i^r$, the angle bending energy $U_i^\varphi$ and the dihedral angle torsional potential energy $U_i^\tau$. The total potential energy $U$ of an MT reads

$$U_{bonds}=\sum_{i=1,2}\left(\sum U_i^r+\sum U_i^\varphi+\sum U_i^\tau\right) \tag{2}$$

where $i$ denotes the types of bonds mentioned above（$i$=1 for the intra-PF bonds and $i$=2 for the inter-PF bonds）. The expressions for the three types of bond energy are as follows.

$$U_i^r=\frac{1}{2}k_i^r(\Delta r_i)^2,\ U_i^\varphi=\frac{1}{2}k_i^\varphi(\Delta\varphi_i)^2,\ U_i^\tau=\frac{1}{2}k_i^\tau(\Delta\Phi_i)^2,(i=1,2) \tag{3}$$

Here, $\Delta r_i$ is the change of bond length, $\Delta\varphi_i$ is the change of in-plane bond angle, $\Delta\Phi_i$ is the change of out-of-plane angle, $k_i^r$ is the force constant for bond stretching, $k_i^\varphi$ is the force constant for bond angle bending and $k_i^\tau$ is the force constant for bond torsion. The values of these force constants can be obtained in atomistic simulations or experiments.

In addition, the total potential energy of the MSM model can be written as:

$$U_{beams}=\sum_{i=1,2}\left(\sum U_i^A+\sum U_i^M+\sum U_i^T\right) \tag{4}$$

where, $U_i^A$ is the strain energies of a beam in tension. $U_i^M$ is the strain energy due to bending and $U_i^T$ is the strain energy due to torsion. Here $i$ specifies the quantities of beam $i$ ($i$=1 for longitudinal beams and $i$=2 for lateral beams). The beam energy can be calculated by using the formulae below.

$$U_i^A=\frac{1}{2}\frac{Y_iA_i}{l_i}(\Delta l_i)^2,\ U_i^M=\frac{1}{2}\frac{Y_iI_i}{l_i}(2\Delta\alpha_i)^2,U_i^T=\frac{1}{2}\frac{S_iJ_i}{l_i}(\Delta\beta_i)^2,(i=1,2) \tag{5}$$

Here, $\Delta l_i$ is the length change of the beam, $\Delta\alpha_i$ is the bending angle, $\Delta\beta_i$ is the torsion angle, $Y_i A_i$ is the extensional stiffness, $Y_i I_i$ is the bending stiffness $S_iJ_i$ is the torsional stiffness of the beam.

The equivalency of the MT structure and its MSM model can be established when the

corresponding energy in Eqs. 3 and 5 are equal, which leads to the following relationship between the force constants of the bonds and the stiffnesses of the space beams.

$$\frac{Y_i A_i}{l_i} = k_i^r,\ \frac{Y_i I_i}{l_i} = k_i^\varphi,\ \frac{S_i J_i}{l_i} = k_i^\tau, (i=1,2) \quad (6)$$

In this study the values of $k_i^r$, $k_i^\varphi$, $k_i^\tau$ were obtained from the molecular dynamics simulations [15, 26, 33], i.e., $k_1^r$=3nN/nm, $k_1^\varphi$=2nN·nm, $k_1^\tau$= 0.04nN·nm, $k_2^r$=14nN/nm, $k_2^\varphi$=8.5nN·nm, $k_2^\tau$=0.17nN·nm. The mass of monomer was taken as $M_{mono}$= 55kDa [16, 34].

In structural mechanics [35, 36], the vibration of an MT modeled as the above frame structure is governed by the following dynamic equation.

$$[M]\{\ddot{\chi}\}+[K]\{\chi\}=\{0\} \quad (7)$$

where $[M]$ denotes the global mass matrices of the established frame structure, $[K]$ denotes the stiffness matrices, $\{\ddot{\chi}\}$ denotes the acceleration vector and $\{\chi\}$ denotes the nodal displacement vector. The mode shape and angular frequency $\omega$ (frequency $f=\omega/2\pi$.) of MT vibration can then be obtained by solving the eigenvalue problems defined by the equation below [16]. The calculation was implemented via the Block Lanczos algorithm [37].

$$([K]-\omega^2[M])\{\chi\}=\{0\} \quad (8)$$

The details about the mass and stiffness matrices of the frame structure in Eqs.7 and 8 can be found in an appendix attached.

### 2.2 MSM simulation on MT vibration

To examine the effect of structural details (especially the helicity) on MT vibration, MTs with different $N$ and $S$ were considered in the present study. Their structural details were tabulated in Table 1 including an imaginary (non-helical) MT with $N$ = 13 but $S$ = 0. During

these simulations, two different boundary conditions were considered, i.e. (1) two ends of the MTs were fixed and (2) one end is fixed and the other is free. The fixed boundary condition was implemented by imposing the translational restraints $U_x=0$, $U_y=0$, $U_z=0$ ($U_x$, $U_y$ and $U_z$ are displacements in $x$, $y$ and $z$ directions) and rotational restraints $ROT_x=0$, $ROT_y=0$, $ROT_z=0$ ($ROT_x$, $ROT_y$, $ROT_z$ are rotation angles about x, y and z axes) on the nodes in a region close to MT ends.

## 3. Results and discussions

In this section, the MSM model introduced in the prior section was employed to perform simulations on the vibration of MTs with different configurations. The focus was placed on the unique features of MT vibration and the effect of structural details on the dynamic behaviors, such as the number of PFs, the helix-start number S and the characteristic length.

### 3.1 3D transverse vibration of MTs

Herein, the transverse vibrations were simulated for long 13-3 MTs (i.e., $N$=13 and $S$ = 3) with two fixed ends and the length-to-diameter ratio $L/D$ =113 or the contour length $L$=2.4μm. Its fourth vibration mode (i.e., the axial half wave number $m$ = 4) was shown in a three-dimensional (3D) graph and projected to the three coordinate planes in Fig. 2. For the sake of comparison, the fourth mode was also shown for a non-helical 13 MT (i.e., $N$ =13 and $S$ = 0) with the same end conditions and the same length. It should be pointed out that the non-helical MT does not exist. It is an MSM model created merely for the comparison.

As listed in Table 2, the frequencies of the 13-3 MTs and the non-helical MSM model

were almost the same, indicating that the helicity did not significantly affect the natural frequency of MTs. Thus, in what follows we focused our attention on the mode shapes of the transverse vibration shown in Fig. 2. It is seen from the figure that the vibration modes and their projections in the YOZ and XOZ planes are quite similar between the 13-3MT and its non-helical counterpart. On the other hand, a substantial difference was identified in the projections on the YOX plane, i.e., one straight line was observed for the non-helical MT, suggesting that the whole tube is vibrating in the same plane. This behavior was very similar to the one achieved for classical beams. Concurrently, four different straight lines were found in the XOY plane of the 13-3MT, showing that its four half waves are vibrating in four different planes. Thus, Fig.2 showed a 3D transverse vibration for 13-3 MTs.

To confirm the observation in Fig. 2 the vibration mode with $m = 4$ was further enlarged in Fig. 3 for the two types of the nanoscale tubules. Herein Fig. 3a clearly indicated that the 13 MT ($S = 0$) is oscillating in a single plane, i.e., all the four half waves stay in the same oscillation plane. In contrast, Fig. 3b demonstrated that for 13-3 MTs the half wave plane rotates in an anticlockwise direction. The rotation angles between adjacent planes are denoted by $\xi_1$, $\xi_2$ and $\xi_3$, respectively. It is understood that bending plays an important role in the transverse vibration of MTs. Thus the spin of the half wave planes suggested the rotation of the bending axis of MT cross section as the directions of oscillation and the bending axis are always perpendicular to each other. It should be noted that Fig.3b only gave a simplified model of the vibration. More detailed study showed that for 13-3MTs individual half waves do not really oscillate in the same plane. As can be seen in Fig. 3c, the anticlockwise rotation of the bending axis actually occurs continuously throughout the whole length of the MT.

To correlate the rotation of the oscillation planes and their bending axis we set up a Cartesian coordinate system on the MT (Fig. 3c) where the origin coincides with the cross section center on the left end, *oz* represents the longitudinal direction and *oy* shows the bending axis on the left end. Next let us consider the cross section at the middle point of the first half wave. The rotation angle $\delta_1$ of its bending axis relative to the *oy* was utilized to characterize the average rotation of the 1st half wave plane (or oscillation plane 1 in Fig. 3). Subsequently, we defined $\delta_2$ , $\delta_3$ and $\delta_4$ in a similar way for the 2nd, 3rd and 4th half waves to measure the average rotation of the oscillation planes 2, 3 and 4, respectively (Fig. 3c). The relative rotation angles $\xi_1$, $\xi_2$ and $\xi_3$ between the two adjacent oscillation planes shown in Fig. 3b were defined by $\xi_1=\delta_2-\delta_1$, $\xi_2=\delta_3-\delta_2$ and $\xi_3=\delta_4-\delta_3$. Thus, the total rotation angle $\xi_{all}$ is given by $\xi_{all}=\xi_1+\xi_2+\xi_3=\delta_4-\delta_1$.

It is noted in the simulations that the rotation of oscillation planes was not uniformly distributed along the axial direction, for instance, the angles $\xi_1$, $\xi_2$, $\xi_3$ of 13-3 MT ($L$=800 *nm*, $m$=4) were measured as 3.79°, 2.58°, 3.53° respectively. The results showed that the rotation became more pronounced at the two ends of the MT. In addition, the total rotation angle $\xi_{all}$ increased as the half wave number $m$ became larger, for instance, $\xi_{all}$ of the aforementioned MT was 2.32°, 5.35° and 9.9° for $m$ = 2, 3 and 4, respectively. This issue was discussed in more detail in Sec. 3.2. Here it should be emphasized that, as shown above, the frequency and thus the energy of the vibration did not change significantly in the presence of the oscillation plane rotation. This suggested that no significant torsion occurred for the vibrating MTs. The rotation of the oscillation plane is merely due to the continuous rotation of the bending axis on the cross sections when $z$ increases from 0 to $L$ (MT length) (Fig. 3c).

To find a possible explanation of the observed phenomenon we restored to the bending theory of Euler beam model [38] as bending occurs for the MT in the transverse vibration. Thus, the vibration frequency is determined by the second moment of inertia *I* of the MT cross section. However, as shown in Fig. 4a-c, due to the helical structure of 13-3 MTs the material is not uniformly distributed along the perimeter of the MT cross section. In particular, the distribution varied with the *S* index as shown in Fig. 4e and was also found to change or rotate from cross section A to its adjacent cross section B. It is understood that the frequency was exactly the same everywhere on the MT, suggesting that the value of the inertia *I* on the individual cross sections of the MT should be nearly the same. Consequently, the different material distribution on the adjacent cross sections finally led to the rotation of the bending axis between the two adjacent cross sections to maintain the identical inertia *I* and accordingly, the same vibration frequency. Thus, the helical structure of MT can at least partially explain the physical mechanisms of the 3D transverse vibration. Here we are very keen to find direct evidence to confirm the existence of the 3D transverse vibration of MTs. Unfortunately, the experimental data are still not available in the literature. On the other hand, it is noted that this vibration mode is similar to the 3D bending reported for cantilevered MTs based on a finite element model in [39]. The finite element simulations can to some extent support the present study where the 3D transverse vibration was observed.

## 3.2 Factors influencing the 3D vibration

The novel 3D transverse vibration mode was achieved in the previous section for 13-3 MTs. In this section, we further examined the effect of the major factors that may exert

significant effects on this vibration mode or the rotation angle. The factors can be categorized into two groups including the internal factors, i.e., the structural details of MTs and the external factors, such as length, vibration modes and the boundary conditions.

### 3.2.1 Internal factors

To examine the effect of MT structures 10 MTs with different *N*-*S* parameters were considered (Table 1) and the rotation angle $\xi_{\text{all}}$ defined in Sec.3.1 and shown in Fig. 3c was calculated for the 4th mode of these sample MTs. The results were shown as a function of helix-start *S* in Fig. 5a and *PF* number *N* in Fig. 5b, respectively. It is noted in Fig. 5a that the angle increases linearly with rising *S*. The slope of the curve is around 1.42° / per unit *S*. Fitting the data in Fig. 5a yielded the following linear relation between the total rotation angle $\xi_{\text{all}}$ and the helix start number *S*, showing a strong dependency of $\xi_{\text{all}}$ on the helical structures of MTs.

$$\xi_{all}=-0.195+1.422\cdot S \quad (S = 1, 2, 3) \tag{9}$$

These results provided clear evidence that, as commented in Sec.3.1 the helical structures of MTs should be responsible for the rotation of the oscillation planes or the bending axis of the cross sections shown in Fig. 3. On the other hand, it is seen from Fig. 5b that, for a given *S* the angle $\xi_{\text{all}}$ remains nearly a constant independent of the *PF* number *N*. Thus, the *PF* number *N* does not exert significant influence on the rotation angle directly. Here it is noted that, for 13MTs with skew angle $\theta = 0$ Eq. 1 reduces to $r = \frac{Sa}{N}$. Thus when *S* is fixed and *N* changes, while the rotation angle remains constant, the subunit rise *r* and also the helical angle $\frac{r}{\delta x}$ will change substantially. Here $\delta x$ is the PF separation (Fig.1). From these analyses it follows that the rotation of the bending axis is independent of the subunit rise or the helical angle of MTs.

It is primarily controlled by the helicity start number *S* describing the periodic change of structure in the axial or *PF* direction.

Furthermore, in Fig. 6 we calculated the frequency for the MTs considered in Fig. 5. The results showed that the frequency generally increased with rising *N* or the diameter of MTs. This *N*-dependency turned out to be more significant for higher modes with larger *m*. On the contrary, for a given *N* the frequency of all the modes selected remains unchanged when the helical start number *S* varying between 2 to 4. These results are found to be consistent with the results obtained previously in [16].

### 3.2.2 External factors

In addition to the MT structures there also exist some external factors that may affect the rotation angle. These factors may include the contour length (or wavelength) of MTs, the mode number of the vibrations and the boundary conditions on the two ends of MTs. It is thus of interest to measure their effects on the rotation angle $\xi_{all}$ for MTs. To this end we calculated the angle $\xi_{all}$ of 13-3 MTs with different lengths. The results obtained for the 3 modes with *m* = 2, 3, 4 were plotted in Fig.7 against the contour length of MTs. As shown in the figure, for a given vibration mode the angle $\xi_{all}$ decreases monotonically with the increasing contour length. The rate of change increases when the contour length becomes shorter. The second order polynomial fitting for *m* = 2, 3, 4 was also given in Fig. 7 with R-square of 0.89045, 0.98056, 0.98496, respectively.

In addition, Fig. 7 indicated that, for a given contour length the rotation angle $\xi_{all}$ increases with rising mode number *m.* The rate of change in angle $\xi_{all}$ is found to increase with

decreasing contour length. As mentioned above, when the contour length decreases or the mode number $m$ increases the rotation angle $\xi_{all}$ becomes greater. This can be attributed to the fact that the (half) wave length declines in these two processes. Thus we came to the conclusion that the rotation angle $\xi_{all}$ is larger for the vibration with a shorter wave length. Further it was seen from Fig. 7 that, for the same wave length the total rotation angle $\xi_{all}$ increases with increasing half wave number $m$. For example, in Fig. 7 MT vibrations with ($m$, $L$) = (2, 1000$nm$), ($m$, $L$) = (3, 1500$nm$) and ($m$, $L$) = (4, 2000$nm$) have the same half wave length 500$nm$ but the corresponding rotation angle $\xi_{all}$ increases from 1.58°, to 2.96° and to 3.99° when $m$ rises from 2 to 3 and to 4. This showed the relation between the rotation angle $\xi_{all}$ and the half wave number $m$ when the half wave length is kept constant. It is thus evident that, for a fixed (half) wavelength $\xi_{all}$ increases with rising $m$ and thus growing contour length. The decrease of $\xi_{all}$ with rising length observed in Fig. 7 is due to the fact that for a given $m$ the (half) wavelength increases with growing contour length. It is thus evident that the key external factors determining the rotation angles are the (half) wavelength and half wave number (or mode number) $m$ rather than the contour length.

Another external factor that may significantly alter the rotation angle of $\xi_{all}$ is the constrains imposed on the two ends of MTs. To examine the boundary condition effects, we considered the transverse vibration of the 13-3 MTs with the same the contour length 1200$nm$ but two different boundaries conditions, i.e., (1) the two ends are fixed (i.e., fixed-fixed condition) and (2) one end is fixed and the other free (i.e., cantilever condition). The shapes of mode 4 ($m$ = 4) were shown in Fig.8 for the MTs and the rotation angle $\xi_{all}$ measured for the MTs were 6.63±0.09° and 6.15±0.09°, respectively, when fixed-fixed and cantilever boundary

conditions are considered. When mode number decreases from 4 to 3 and 2, the angle associated with fixed-fixed ends decreases from 6.63±0.09° to 3.62±0.09° and 1.31±0.09°. Those obtained for the cantilever boundary condition declines from 6.15±0.09° to 3.16±0.09° and to 1.19±0.09°. These results clearly showed that the fixed-fixed ends lead to the rotation angles significantly larger than those associated with the cantilever boundary condition. In other words, the rotation of the bending axis of the cross section would become more substantial when more constrains are enforced on the two ends of MTs.

As shown above, the 3D transverse vibration mode is achieved as a result of the helix structures of MTs. This shows clear evidence that the unique structures of MTs lead to a deformation pattern significantly different from that of an elastic beam. The new finding is a step forward in gaining an in-depth understanding of the mechanisms via which the MT structures deform in a unique way to fulfill their functions in various physiological processes. The vibration mode-structure relation may also provide useful guidance for the development of the MT-based biomimetic materials whose performance depends heavily on its transverse vibration. Herein, another thing worth mentioning is the damping effect of cytosol, which has to be taken into consideration for MTs in vivo. This issue has not been discussed here as this work is focused on the structure-property relation of individual MTs, e.g., MTs in vitro. The damping effect however deserves to be examined in details in future studies.

## 4. Conclusions:

A unique transverse vibration of MTs is achieved via a recently developed MSM model.

In sharp contrast to the vibration of classical beams, the bending axis of the cross section of vibrating MTs rotates throughout the length of the MTs. As a result, the adjacent half-waves vibrate approximately in two different oscillation planes, showing a 3D transverse vibration for MTs. Nevertheless, no real torsion occurs for the MTs and thus the frequency remains nearly the same in the absence or presence of the bending axis rotation.

In addition, the rotation angle was found to increase almost linearly with the increasing helical start number $S$ but remains independent of the $PF$ number $N$. These indicate that the helical structures of MTs are responsible for the 3D transverse vibration of MTs, and the rotation angle of the bending axis is primarily determined by the periodic arrangement of protein monomers in the axial direction. The helical angle, however, does not play a significant role in determining the rotation angle of the bending axis on MT cross sections.

Furthermore, the wavelength of vibration is identified as a characteristic length that can significantly change the rotation angle of the bending axis. The angle is found to rise with the decreasing wavelength or the growing wavenumber (for a given contour length). Additionally, the rotation angle can be further raised by imposing more constraints on MT ends.

**Acknowledgments**

S. Li acknowledges the support from the China Scholarship Council (CSC).

**References**

[1] Howard J., Hyman A.A. Dynamics and mechanics of the microtubule plus end. Nature.

2003;422:753-8.

[2] Hawkins T., Mirigian M., Yasar M.S., Ross J.L. Mechanics of microtubules. J Biomech. 2010;43:23-30.

[3] Meurer-Grob P., Kasparian J., Wade R.H. Microtubule structure at improved resolution. Biochemistry. 2001;40:8000-8.

[4] Weaver W., Gere J.M. Matrix Analysis Framed Structures: Springer Science & Business Media; 2012.

[5] Wade R. Microtubule structure and dynamics. Curr Opin Cell Biol. 1997;9:12-7.

[6] Chretien D., Wade R.H. New data on the microtubule surface lattice. Biol Cell. 1991;71:161-74.

[7] Chretien D., Fuller S.D. Microtubules switch occasionally into unfavorable configurations during elongation. J Mol Biol. 2000;298:663-76.

[8] Janson M.E., Dogterom M. A bending mode analysis for growing microtubules: evidence for a velocity-dependent rigidity. Biophys J. 2004;87:2723-36.

[9] Howard J., Clark R. Mechanics of motor proteins and the cytoskeleton. Appl Mech Rev. 2002;55:B39.

[10] Wang C.Y., Ru C.Q., Mioduchowski A. Vibration of microtubules as orthotropic elastic shells. Phys E. 2006;35:48-56.

[11] Wang C.Y., Ru C.Q., Mioduchowski A. Orthotropic elastic shell model for buckling of microtubules. Phys Rev E. 2006;74:052901.

[12] Wang C.Y., Zhang L.C. Circumferential vibration of microtubules with long axial wavelength. J Biomech. 2008;41:1892-6.

[13] Wang C.Y., Li C.F., Adhikari S. Dynamic behaviors of microtubules in cytosol. J Biomech. 2009;42:1270-4.

[14] Wang C.Y., Guo Z.G., Wang R.J., Luo Y. Role of the inter-protofilament sliding in the bending of protein microtubules. J Biomech. 2016.

[15] Zhang J., Wang C.Y. Molecular structural mechanics model for the mechanical properties of microtubules. Biomech Model Mechan. 2014;13:1175-84.

[16] Zhang J., Wang C.Y. Free vibration analysis of microtubules based on the molecular mechanics and continuum beam theory. Biomech Model Mechan. 2015:1-10.

[17] Xiang P., Liew K.M. Predicting buckling behavior of microtubules based on an atomistic-continuum model. Int J Solids Struct. 2011;48:1730-7.

[18] Tounsi A., Heireche H., Benhassaini H., Missouri M. Vibration and length-dependent flexural rigidity of protein microtubules using higher order shear deformation theory. J Theor Biol. 2010;266:250-5.

[19] Allen K.B., Sasoglu F.M., Layton B.E. Cytoskeleton-membrane interactions in neuronal growth cones: a finite analysis study. J Biomech Eng. 2009;131:021006.

[20] Ji X.Y., Feng X.Q. Mechanochemical modeling of dynamic microtubule growth involving sheet-to-tube transition. PLoS One. 2011;6:e29049.

[21] Molodtsov M.I., Ermakova E.A., Shnol E.E., Grishchuk E.L., McIntosh J.R., Ataullakhanov F.I. A molecular-mechanical model of the microtubule. Biophys J. 2005;88:3167-79.

[22] Pokorný J., Vedruccio C., Cifra M., Kučera O. Cancer physics: diagnostics based on damped cellular elastoelectrical vibrations in microtubules. Eur Biophys J. 2011;40:747-59.

[23] Iijima S. Helical microtubules of graphitic carbon. Nature. 1991;354:56-8.

[24] Jishi R.A., Dresselhaus M.S., Dresselhaus G. Electron-phonon coupling and the electrical conductivity of fullerene nanotubules. Phy Rev B. 1993;48:11385.

[25] Pampaloni F., Florin E.L. Microtubule architecture: inspiration for novel carbon nanotube-based biomimetic materials. Trends Biotechnol. 2008;26:302-10.

[26] Zhang J., Meguid S. Buckling of microtubules: An insight by molecular and continuum mechanics. Appl Phys Lett. 2014;105:173704.

[27] Chu J.W., Voth G.A. Allostery of actin filaments: molecular dynamics simulations and coarse-grained analysis. Proc Natl Acad Sci U S A. 2005;102:13111-6.

[28] Hunyadi V., Chretien D., Flyvbjerg H., Janosi I.M. Why is the microtubule lattice helical? Biol Cell. 2007;99:117-28.

[29] Hyman A.A., Chrétien D., Arnal I., Wade R.H. Structural changes accompanying GTP hydrolysis in microtubules: information from a slowly hydrolyzable analogue guanylyl-(alpha, beta)-methylene-diphosphonate. J Cell Biol. 1995;128:117-25.

[30] Hunyadi V., Chretien D., Janosi I.M. Mechanical stress induced mechanism of microtubule catastrophes. J Mol Biol. 2005;348:927-38.

[31] Li C.Y., Chou T.W. A structural mechanics approach for the analysis of carbon nanotubes. Int J Solids Struct. 2003;40:2487-99.

[32] Enemark S., Deriu M.A., Soncini M., Redaelli A. Mechanical model of the tubulin dimer based on molecular dynamics simulations. J Biomech Eng. 2008;130:041008.

[33] Ji X.Y., Feng X.Q. Coarse-grained mechanochemical model for simulating the dynamic behavior of microtubules. Phys Rev E. 2011;84:031933.

[34] Wade R.H. On and around microtubules: an overview. Mol Biotechnol. 2009;43:177-91.

[35] Tedesco J.W., McDougal W.G., Ross C.A. Structural dynamics: theory and applications: Addison-Wesley Montlo Park, California; 1999.

[36] Li C., Chou T.-W. Vibrational behaviors of multiwalled-carbon-nanotube-based nanomechanical resonators. Appl Phys Lett. 2004;84:121-3.

[37] Kim Y.J. Block Lanczos algorithm: Monterey, California. Naval Postgraduate School; 1989.

[38] Gere J.M., Goodno B.J. Mechanics of materials: Nelson Education; 2012.

[39] Kasas S., Kis A., Riederer B.M., Forró L., Dietler G., Catsicas S. Mechanical properties of microtubules explored using the finite elements method. Chemphyschem. 2004;5:252-7.

[40] Dhatt G., Touzot G., Cantin G. The Finite Element Method Displayed. 1984. John Wiley&Sons, Chichester.

## Table captions

Table 1 The structural details of various MTs[7]

Table2 Natural frequencies of different vibration modes of models (MHz)

## Tables

Table 1 The structural details of various MTs[7]

| Parameter | Sym | Value | | | | | | | | | | |
|---|---|---|---|---|---|---|---|---|---|---|---|---|
| Proto-filament number | $N$ | 12 | 12 | 13 | 13 | 14 | 14 | 14 | 15 | 15 | 16 | 13* |
| helix-start number | $S$ | 2 | 3 | 2 | 3 | 2 | 3 | 4 | 3 | 4 | 4 | 0 |
| Proto-Filament separation | $\delta x$ (nm) | 5.18 | 5.27 | 5.02 | 5.13 | 5.08 | 5.16 | 5.05 | 5.07 | 5.06 | 5.19 | 5.13 |
| Subunit repeat | $a$ (nm) | 4.05 | 4.04 | 4.07 | 4.05 | 4.06 | 4.05 | 4.05 | 4.05 | 4.04 | 4.04 | 4.05 |
| skew angle | $\theta$(°) | -1.02 | 0.85 | -1.64 | 0 | -2.34 | -0.68 | 0.87 | -1.33 | 1.81 | 1.17 | 0 |

* Imaginary (non-helical) MT

Table 2 Natural frequencies of different vibration modes of models (MHz)

| Models | | | 13-3 MSM model of MT | Non-helical MSM model |
|---|---|---|---|---|
| Half wave Numbers | m=1 | $\lambda/2D$=113 | 3.4154 | 3.4156 |
| | m=2 | $\lambda/2D$=56.5 | 9.4014 | 9.4019 |
| | m=3 | $\lambda/2D$=37.7 | 18.3960 | 18.3970 |
| | m=4 | $\lambda/2D$=28.25 | 30.3360 | 30.3390 |

## Figure captions

Fig. 1 Parameterized MT structure and its MSM model; Here $a$ is the subunit repeat, $r$ is the subunit rise, $R$ is the radius of the MT, $\delta x$ is the protofilament separation and $\theta$ is the skew angle of protofilament relative to the direction of the axis of the MT. Vertical blue lines represent the intra-PF bonds of the MT and beam 1 of the MSM model, and the red ones denote the inter-PF bonds of the MT and beam 2 of the MSM model.

Fig. 2 Transverse vibration modes ($m$ = 4) and its the projection to the YOX, YOZ, XOZ planes obtained for (a) an imaginary non-helical 13 MT and (b) a 13-3 MT;

Fig. 3 The simplified mode shape ($m$ = 4) for (a) an imaginary 13MT and (b) a 13-3 MT where the rotation of the half wavelength planes (or oscillation planes) is shown. The real mode shape of the 13-3MT is shown in (c) where the bending axis rotates throughout the whole length of the MT.

Fig. 4 The material distribution on the perimeter of MTs with different S.

Fig. 5 Dependence of the rotation angle $\xi_{all}$ ($L$=2000nm) on (a) the helical start number S and (b) the number of protofilaments $N$ obtained for the 4$^{th}$ model of the MT vibration.

Fig. 6 The effect of structural details on the frequency of MTs with different S and N. Here the half wave number $m$ changes from 1 to 4.

Fig. 7 The length dependenence of the angle $\xi_{all}$ of standard 13-3 MTs

Fig. 8 Mode shapes of a vibrating MT with (a) fixed-fixed ends and (b) fixed-free ends; The YOX projections of the mode shapes are shown in (c) and (d), respectively.

Figures

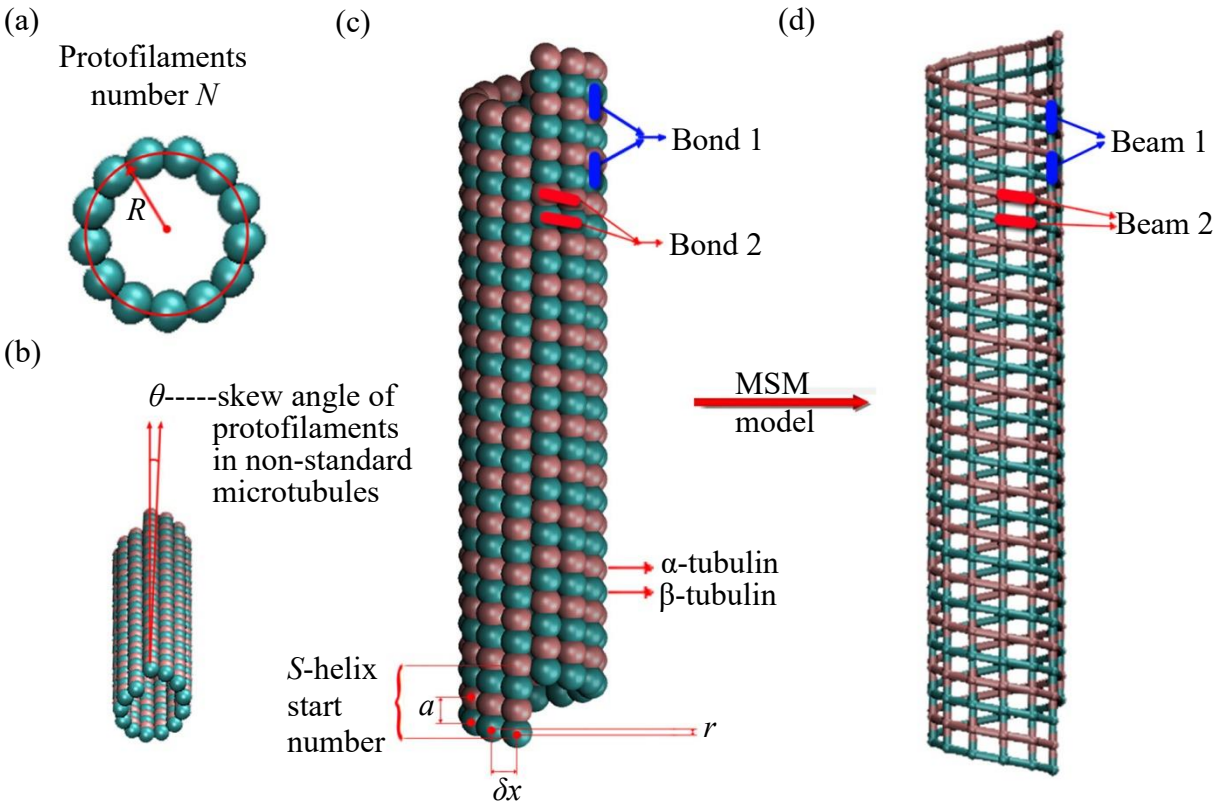


Fig. 1 Parameterized MT structure and its MSM model; Here $a$ is the subunit repeat, $r$ is the subunit rise, $R$ is the radius of the MT, $\delta x$ is the protofilament separation and $\theta$ is the skew angle of protofilament relative to the direction of the axis of the MT. Vertical blue lines represent the intra-PF bonds of the MT and beam 1 of the MSM model, and the red ones denote the inter-PF bonds of the MT and beam 2 of the MSM model.

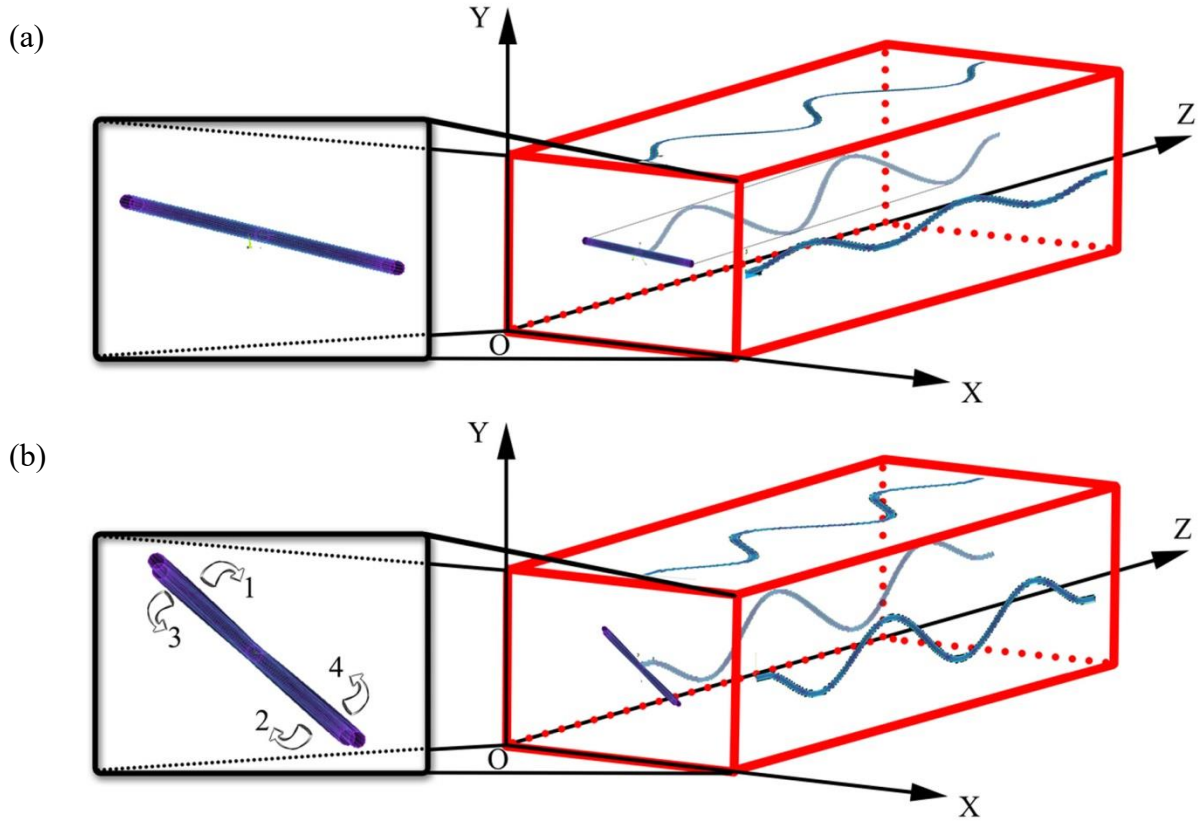


Fig. 2 Transverse vibration modes ($m$ = 4) and its the projection to the YOX, YOZ, XOZ planes obtained for (a) an imaginary non-helical 13 MT and (b) a 13-3 MT;

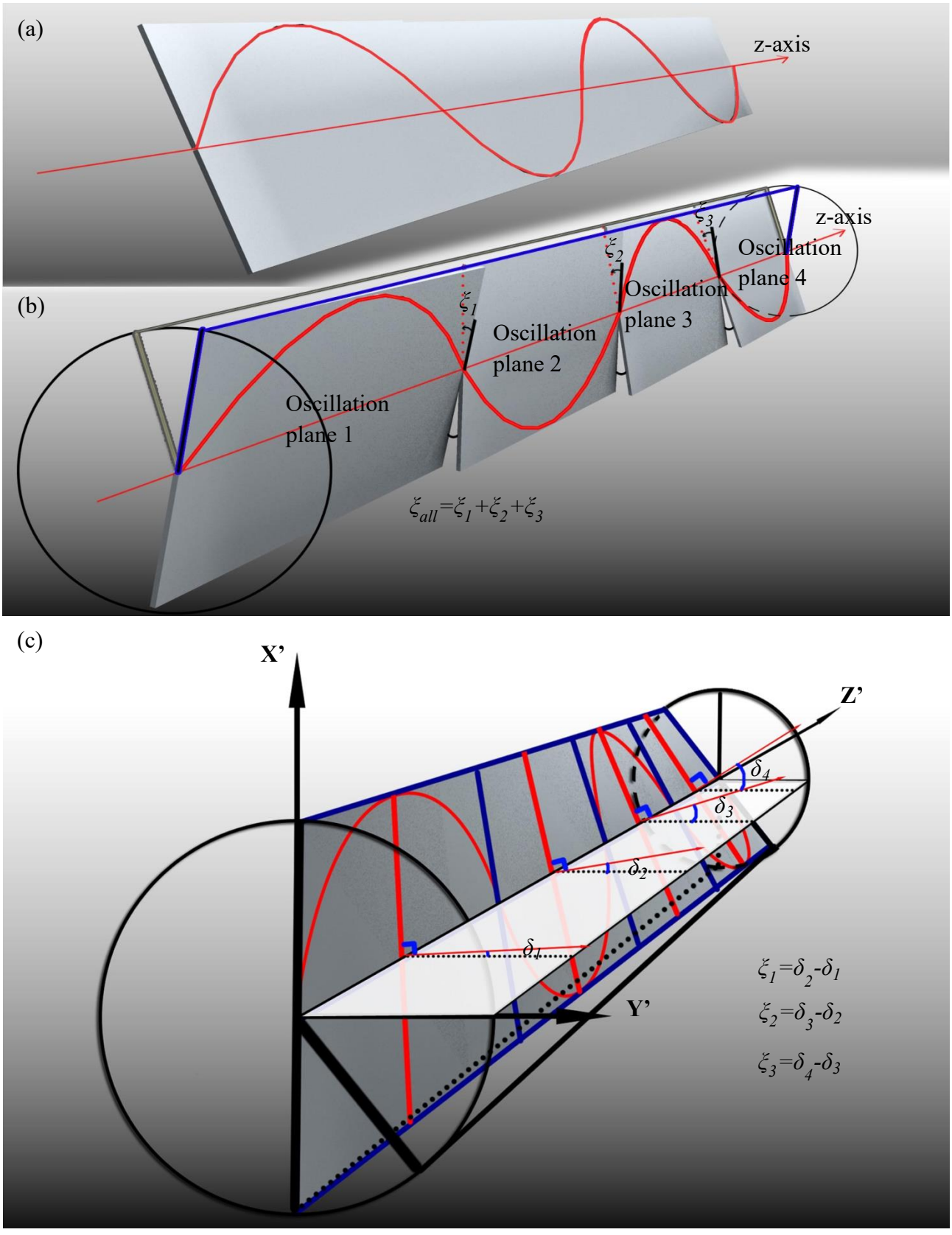


Fig. 3 The simplified mode shape ($m$ = 4) for (a) an imaginary 13MT and (b) a 13-3 MT where the rotation of the half wavelength planes (or oscillation planes) is shown. The real mode shape of the 13-3MT is shown in (c) where the bending axis rotates throughout the whole length of the MT.

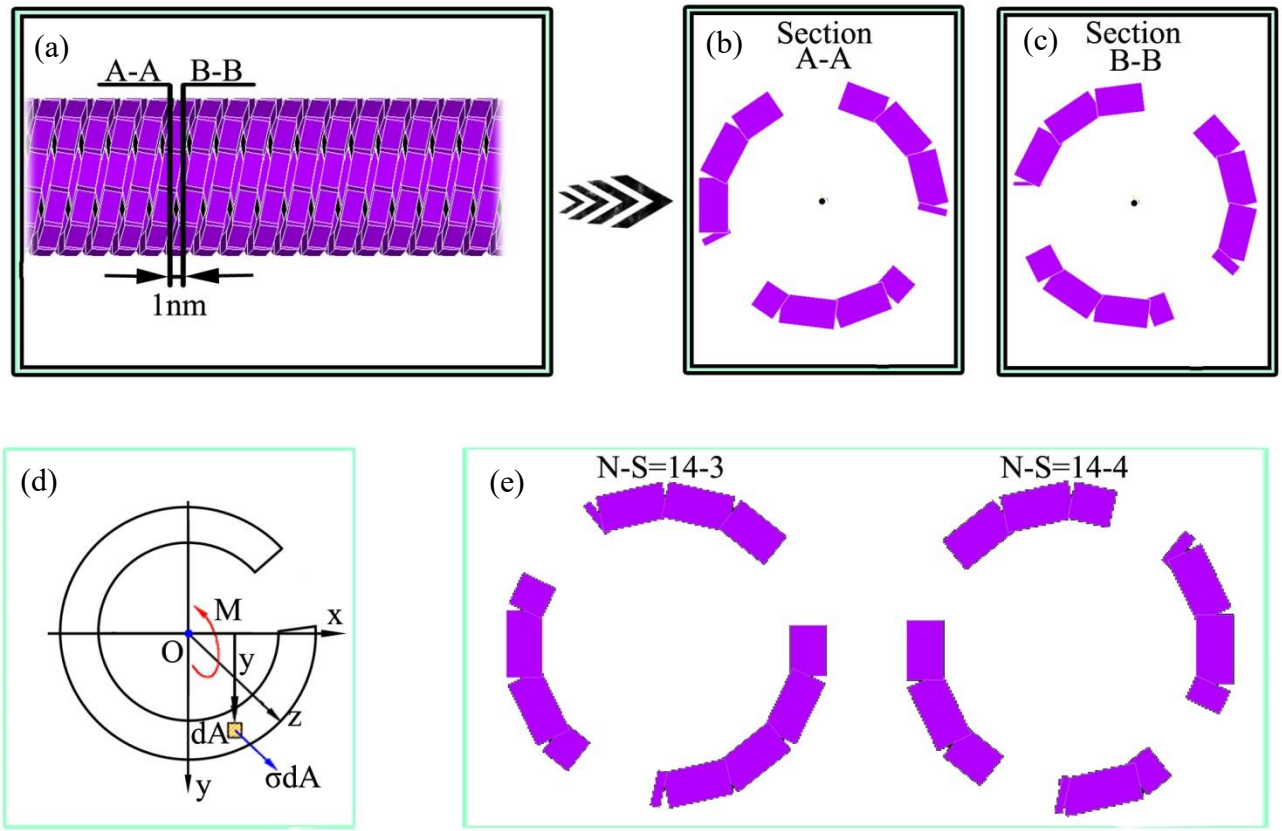


Fig. 4 The material distribution on the perimeter of MTs with different S.

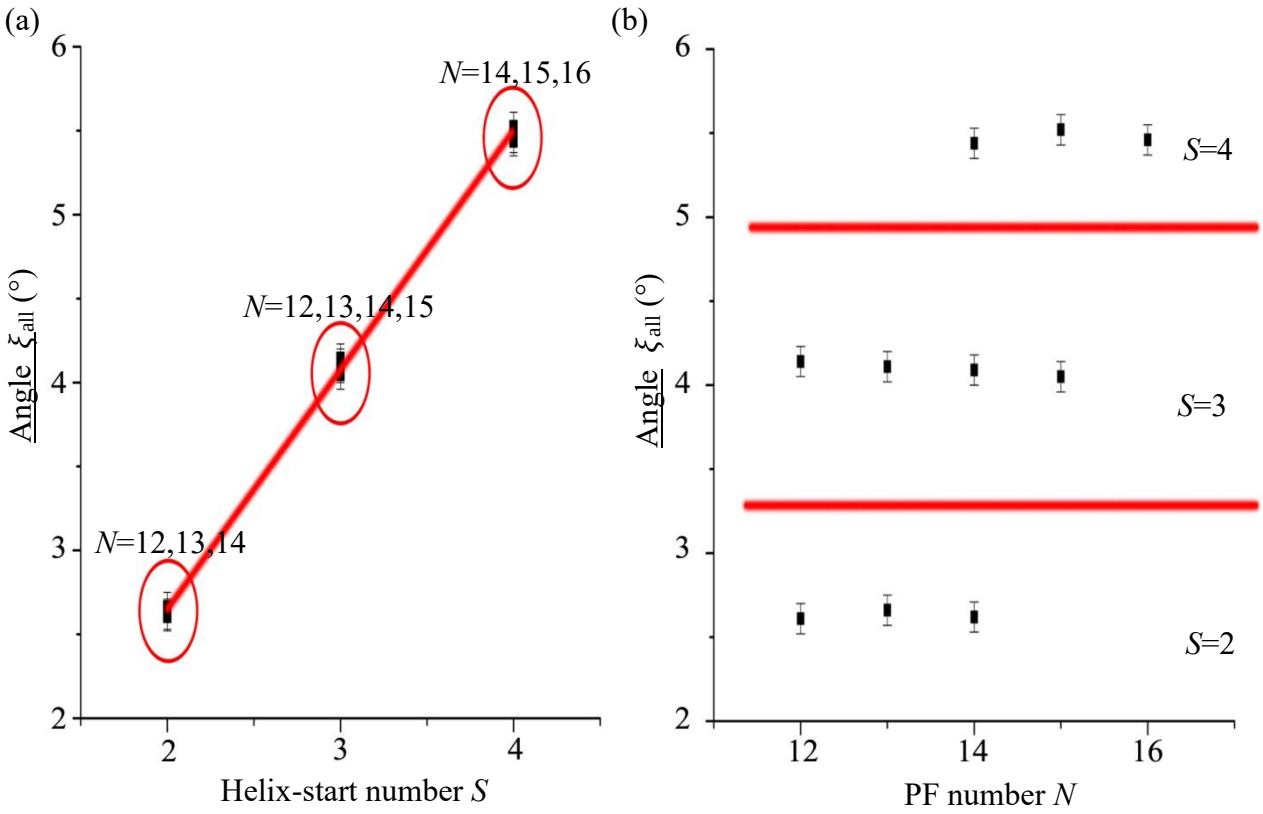


Fig. 5 Dependence of the rotation angle $\xi_{all}$ ($L$=2000nm) on (a) the helical start number S and (b) the number of protofilaments $N$ obtained for the 4$^{th}$ model of the MT vibration.

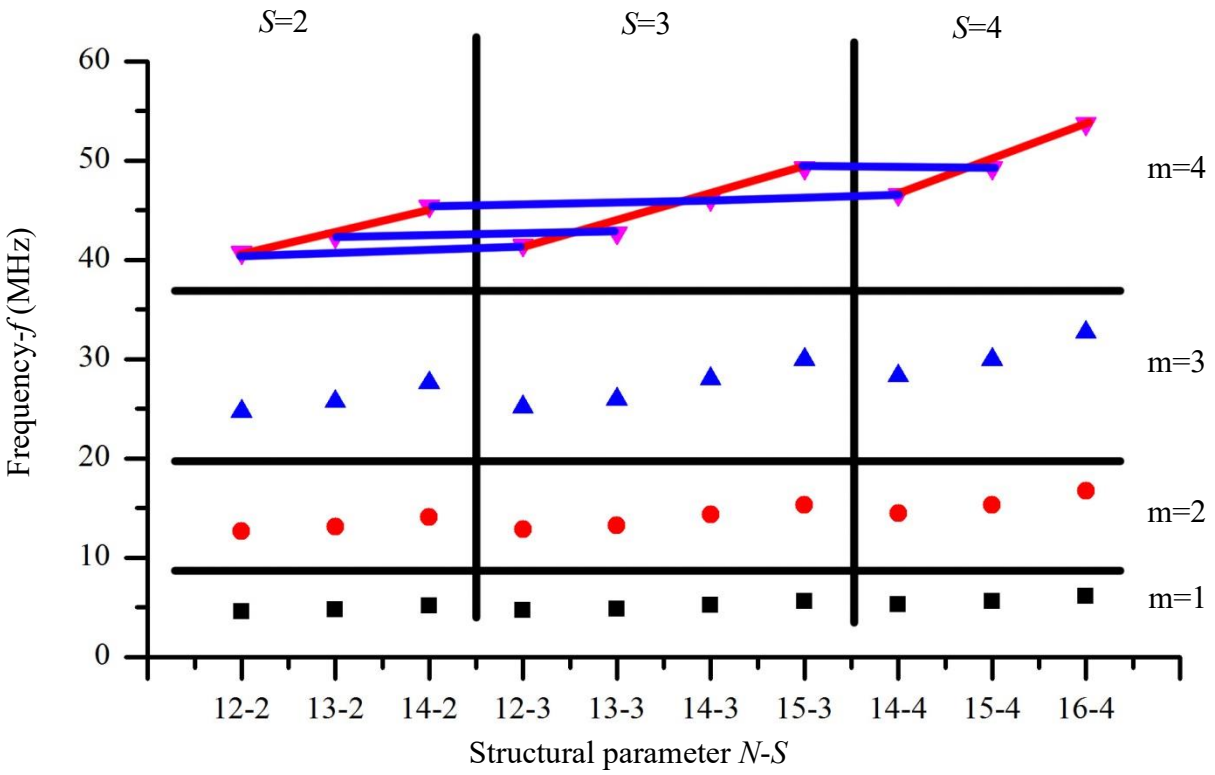


Fig. 6 The effect of structural details on the frequency of MTs with different S and N. Here the half wave number *m* changes from 1 to 4.

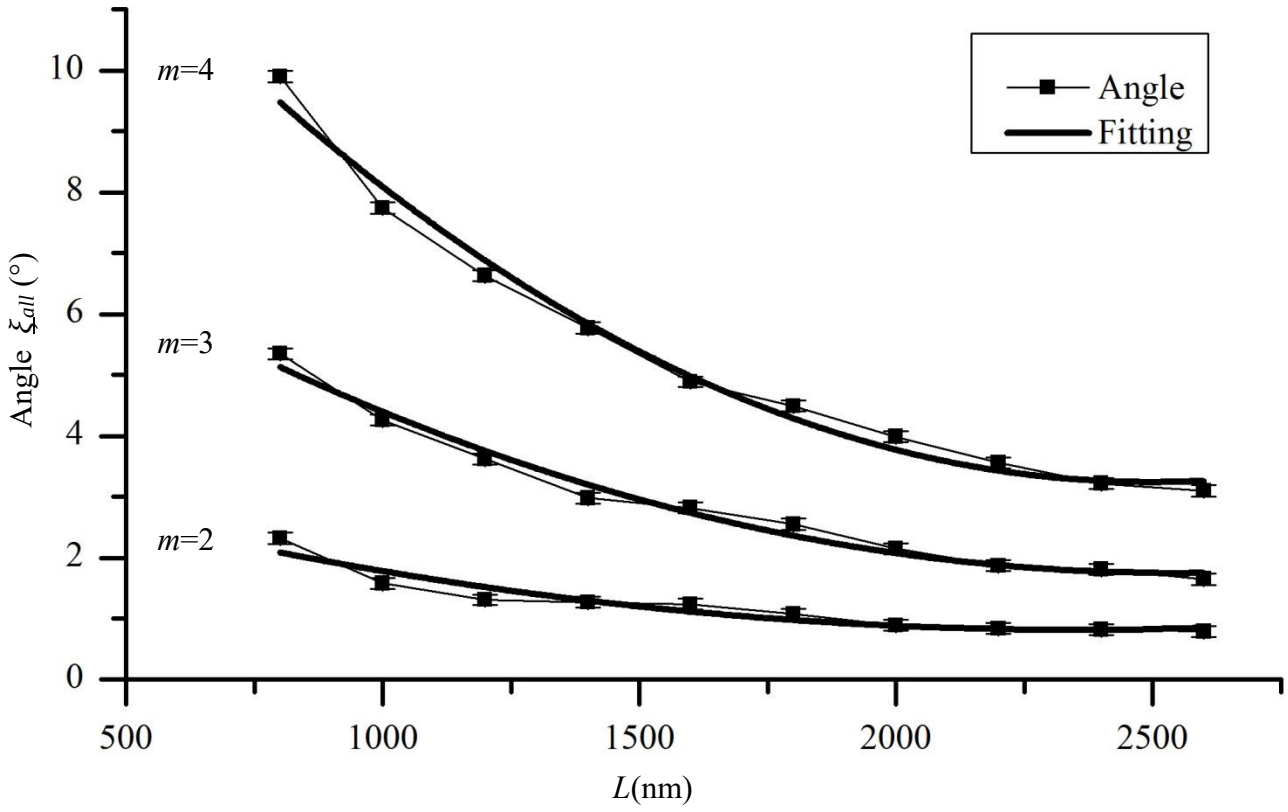


Fig. 7 The length dependenence of the angle $\xi_{all}$ of standard 13-3 MTs

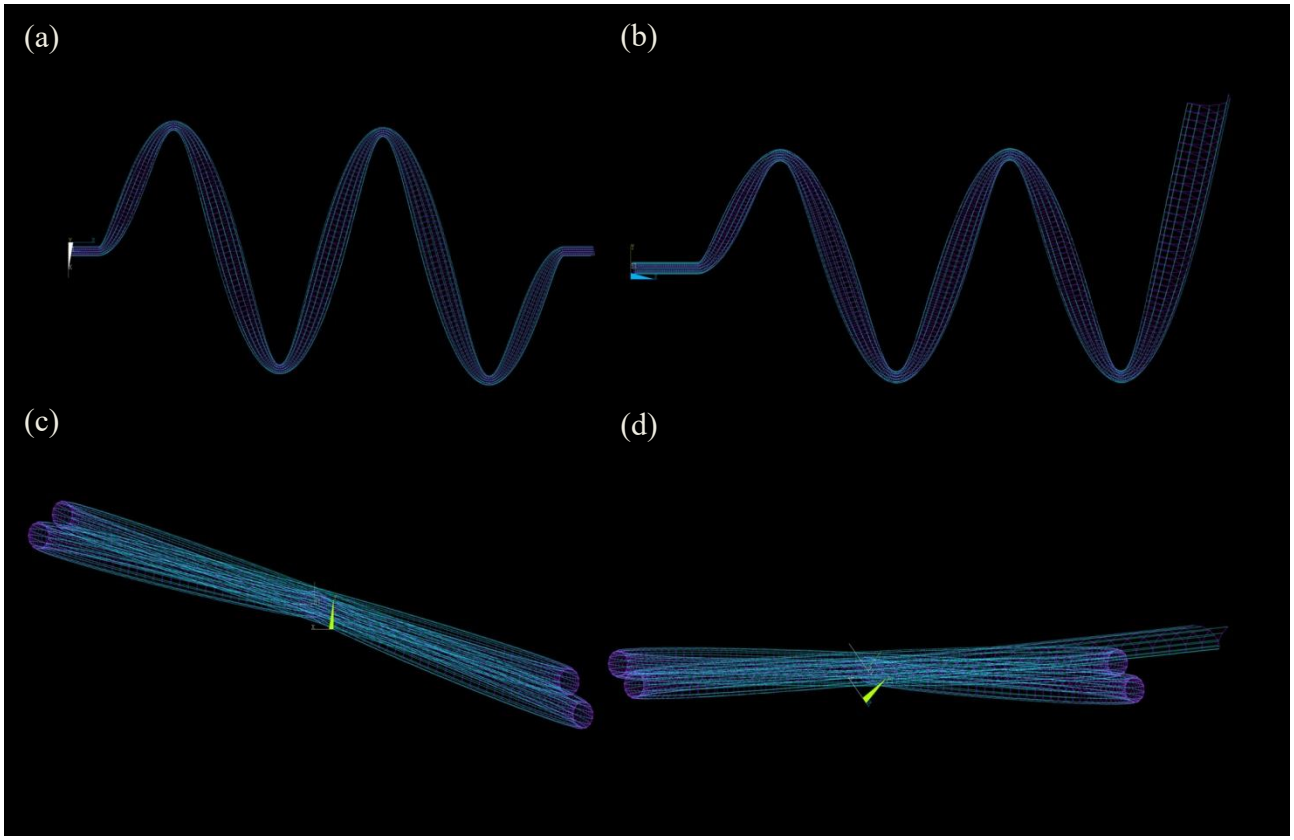


Fig. 8 Mode shapes of a vibrating MT with (a) fixed-fixed ends and (b) fixed-free ends; The YOX projections of the mode shapes are shown in (c) and (d), respectively.